Journal of Systems Engineering and Electronics
Vol. 31, No. 4, August 2020, pp.703 – 711

Exponential time differencing based efficient SC-PML for RCS simulation

NIU Liqiang[1], XIE Yongjun[1], JIANG Haolin[2,*], and WU Peiyu[1]

1. School of Electronic and Information Engineering, Beihang University, Beijing 100191, China;
2. School of Information Science and Engineering, Southeast University, Nanjing 210096, China

Abstract: To efficiently simulate and calculate the radar cross section (RCS) related electromagnetic problems by employing the finite-difference time-domain (FDTD) algorithm, an efficient stretched coordinate perfectly matched layer (ESC-PML) based upon the exponential time differencing (ETD) method is proposed. The proposed implementation can not only reduce the number of auxiliary variables in the SC-PML regions but also maintain the ability of the original SC-PML in terms of the absorbing performance. Compared with the other existed algorithms, the ETD-FDTD method shows the least memory consumption resulting in the computational efficiency. The effectiveness and efficiency of the proposed ESC-PML scheme is verified through the RCS relevant problems including the perfect E conductor (PEC) sphere model and the patch antenna model. The results indicate that the proposed scheme has the advantages of the ETD-FDTD method and ESC-PML scheme in terms of high computational efficiency and considerable computational accuracy.

Keywords: exponential time differencing (ETD), efficient stretched coordinate (ESC), finite-difference time-domain (FDTD), perfectly matched layer (PML), radar cross section (RCS).

DOI: 10.23919/JSEE.2020.000045

1. Introduction

As one of the most wide spread full-wave analytic procedures in the numerical simulation, the finite-difference time-domain (FDTD) method, proposed by Yee, is deemed as one of the most powerful tools in solving the Maxwell's equations, simulating the wave propagation. With its high computational efficiency, simplicity and wideband capability, the FDTD algorithm has widely application especially in calculating the radar target characteristics. The simulation of radar cross section (RCS) is one of the most significantly problems among various challenges in the radar system. The RCS is the pivotal element in the radar detection and stealth [1]. Consequently, it is important to predict and calculate the RCS accurately. To achieve such ends, a precise RCS evaluation by employing the full-wave numerical simulation is regarded as a frontier science. Among the RCS concepts, the RCS in the far field has raised public concern, especially far field RCS characteristics [2].

When simulating the far field RCS by the FDTD algorithm, the large open region problems must be considered. As the computers cannot simulate the infinite computational domain, the boundary condition must be employed during the calculation [3]. The absorbing boundary condition (ABC) is employed to absorb the outgoing waves and reduce the wave reflection so that the space outside the computational domain becomes lager resulting in the negligible level of the reflection waves in the ABC regions. As one of the most well-known ABCs, the perfectly matched layer (PML), proposed by Bérenger, has been extensively researched [4]. Among several PML implementations, the stretched coordinate PML (SC-PML), proposed by Chew and Weedon, is introduced to simplify its implementation at corners and edges of the PML regions [5]. Since then, several SC-PML schemes have been carried out including the auxiliary differential equation (ADE) method, the bilinear Z transform (BZT) method and the matched Z transform (MZT) method [6 – 8]. However, at least two auxiliary variables are employed in the afore-mentioned schemes, resulting the quite low computational efficiency.

In order to improve the computational efficiency and maintain the computational accuracy, several efficient SC-PML (ESC-PML) implementations have been introduced. In 2006, Li proposed an ESC-PML, denoted as LI-PML, by combining the second-order differential equations with the digital signal processing techniques [9]. However, LI-PML has complicate mathematical derivation due to introducing the higher order equations. The memory consumption still maintains a high level. In 2011, Ramadan proposed an ESC-PML, denoted as OR-PML [10]. Compared with LI-PML, second-order differential equations are re-

Manuscript received February 05, 2020.
*Corresponding author.
This work was supported by the National Natural Science Foundation of China (61571022; 611971022).

placed by first-order equations resulting in lower memory consumption. In 2019, Jiang proposed ESC-PMLs based on the ADE, BZT and MZT methods, denoted as CT-ADE-PML, CT-BZT-PML and CT-MZT-PML, respectively [11,12]. Fewer arithmetic operations and coefficients have been obtained. However, the afore-mentioned methods still have their own limitations. They are not clear as the discretization scheme should be used when high-order derivatives are involved [13]. Thus, the exponential time differencing (ETD) method which involves the exact integration of the governing equations is introduced [14].

Here, the ESC-PML implementation is proposed based on the ETD-FDTD method, denoted as ETD-PML. The proposed ETD-PML obtains the better performance and higher computational efficiency by decreasing the auxiliary variables compared with the existed PMLs including ESC-PMLs and uniaxial PML (UPML) which has widely employed in the commercial software. Compared with the previously works on ESC-PMLs, the proposal can further reduce the operation manipulations. The computational efficiency is verified both in theory and numerical simulation. Through numerical examples including the perfect E conductor (PEC) sphere model and the patch antenna model, the effectiveness of the proposed method has been demonstrated. The results show that the proposed scheme can not only maintain the absorbing performance of SC-PMLs but also decrease the computational resources during the simulation.

2. Formulations

By introducing the generalized material independent concept, the proposed ETD-PML can be independent of the materials [11,12]. Thus, the electric flux density $\boldsymbol{D}$ and the magnetic flux density $\boldsymbol{B}$ are introduced as follows:

$$\boldsymbol{D}(\omega)=\varepsilon_0\varepsilon(\omega)\boldsymbol{E}(\omega) \tag{1}$$

$$\boldsymbol{B}(\omega)=\mu_0\mu(\omega)\boldsymbol{H}(\omega) \tag{2}$$

where ε_0 and μ_0 are the permittivity and permeability of the vaccum, respectively; $\varepsilon(\omega)$ and $\mu(\omega)$ are the relative permittivity and permeability, respectively; $\boldsymbol{E}(\omega)$ and $\boldsymbol{H}(\omega)$ are the electric field intensity and magnetic field intensity, respectively. The Maxwell's equations in the 3-D SC-PML regions can be given as

$$\mathrm{j}\omega\boldsymbol{D}(\omega)=\nabla_s\times\boldsymbol{H}(\omega) \tag{3}$$

$$-\mathrm{j}\omega\boldsymbol{B}(\omega)=\nabla_s\times\boldsymbol{E}(\omega) \tag{4}$$

where

$$\nabla_s=\widehat{x}\frac{1}{S_x}\frac{\partial}{\partial x}+\widehat{y}\frac{1}{S_y}\frac{\partial}{\partial y}+\widehat{z}\frac{1}{S_z}\frac{\partial}{\partial z}. \tag{5}$$

It can be observed that the materials' information can be expressed by employing (3) and (4). Through the calculation of $\boldsymbol{D}$ and $\boldsymbol{B}$, the Maxwell's equations for terminating arbitrary mediums can be renovated by employing the generalized material independent concept.

For simplicity, the x-projection of the Ampere's law is selected as an example. The other components can be updated by employing the same approach. Equation (3) can be rewritten as

$$\mathrm{j}\omega D_x=\frac{1}{S_y}\frac{\partial H_z}{\partial y}-\frac{1}{S_z}\frac{\partial H_y}{\partial z} \tag{6}$$

where D_x is the electric flux density in x-direction; H_y and H_z are the magnetic component in y- and z-directions, respectively; S_η $(\eta=x,y,z)$ is the stretched coordinate variables which can be defined as

$$S_\eta=1+\frac{\sigma_\eta}{\mathrm{j}\omega\varepsilon_0} \tag{7}$$

where σ_η is the PML conductivity profile defined as a function of the distance from the interface of the PML and the computational domain along the η-direction. By multiplying $(\mathrm{j}\omega)^{-1}$ at both sides of (6) and substituting (7) into (6), the result can be written as

$$D_x=\frac{1}{\mathrm{j}\omega+\dfrac{\sigma_y}{\varepsilon_0}}\frac{\partial H_z}{\partial y}-\frac{1}{\mathrm{j}\omega+\dfrac{\sigma_z}{\varepsilon_0}}\frac{\partial H_y}{\partial z} \tag{8}$$

where σ_y and σ_z are the conductivity in the PML region.

By rearranging (8) and auxiliary variables F_x, one obtains

$$D_x+\frac{1}{\mathrm{j}\omega+\dfrac{\sigma_z}{\varepsilon_0}}\frac{\partial H_y}{\partial z}=\frac{1}{\mathrm{j}\omega+\dfrac{\sigma_y}{\varepsilon_0}}\frac{\partial H_z}{\partial y}=F_x. \tag{9}$$

It can be observed that (9) can be splitted into two sub-equations which can be written as

$$\mathrm{j}\omega D_x+\frac{\sigma_z}{\varepsilon_0}D_x+\frac{\partial H_y}{\partial z}=\mathrm{j}\omega F_x+\frac{\sigma_z}{\varepsilon_0}F_x, \tag{10}$$

$$\mathrm{j}\omega F_x+\frac{\sigma_y}{\varepsilon_0}F_x=\frac{\partial H_z}{\partial y}. \tag{11}$$

By employing the relationship $\mathrm{j}\omega\leftrightarrow\dfrac{\partial}{\partial t}$, (10) and (11) can be rewritten as

$$\frac{\partial D_x}{\partial t}+\frac{\sigma_z}{\varepsilon_0}D_x+\frac{\partial H_y}{\partial z}=\frac{\partial F_x}{\partial t}+\frac{\sigma_z}{\varepsilon_0}F_x, \tag{12}$$

$$\frac{\partial F_x}{\partial t}+\frac{\sigma_y}{\varepsilon_0}F_x=\frac{\partial H_z}{\partial y} \tag{13}$$

where t is time variable.

Following the ETD-FDTD method, by multiplying $\mathrm{e}^{\frac{\sigma_y t}{\varepsilon_0}}$ at both sides of (13) and integrating the resultants from the

time step $t=\left(n-\frac{1}{2}\right)\Delta t$ to $t=\left(n+\frac{1}{2}\right)\Delta t$, one obtains

$$F_x^{n+1}=\mathrm{e}^{-\frac{\sigma_y\Delta t}{\varepsilon_0}}F_x^n+$$
$$\mathrm{e}^{-\frac{\sigma_y\Delta t}{\varepsilon_0}}\int_0^{\Delta t}\mathrm{e}^{\frac{\sigma_y\tau}{\varepsilon_0}}\frac{\partial H_z}{\partial y}\times\left[\left(n-\frac{1}{2}\right)\Delta t-\tau\right]\mathrm{d}\tau \quad (14)$$

where τ is the integral variable.

By introducing the linear approximation method to the magnetic components, one obtains

$$\frac{\partial H_z}{\partial y}\times\left[\left(n-\frac{1}{2}\right)\Delta t-\tau\right]=$$
$$\frac{\partial}{\partial y}H_z^{n-\frac{1}{2}}+\tau\frac{\partial}{\partial y}\frac{H_z^{n+\frac{1}{2}}-H_z^{n-\frac{1}{2}}}{\Delta t}. \quad (15)$$

Thus, by substituting (15) into (14), the updated equation of F_x can be written in the FDTD domain as

$$F_x^{n+1}=\mathrm{e}^{-\frac{\sigma_y\Delta t}{\varepsilon_0}}F_x^n+$$
$$\frac{\varepsilon_0^2}{\sigma_y^2\Delta t}\left(\frac{\sigma_y\Delta t}{\varepsilon_0}-1+\mathrm{e}^{-\frac{\sigma_y\Delta t}{\varepsilon_0}}\right)\frac{\partial}{\partial y}H_z^{n+\frac{1}{2}}+$$
$$\frac{\varepsilon_0^2}{\sigma_y^2\Delta t}\left(1-\frac{\sigma_y\Delta t}{\varepsilon_0}\mathrm{e}^{-\frac{\sigma_y\Delta t}{\varepsilon_0}}+\mathrm{e}^{-\frac{\sigma_y\Delta t}{\varepsilon_0}}\right)\frac{\partial}{\partial y}H_z^{n-\frac{1}{2}}. \quad (16)$$

After renovating (16), (12) can be calculated by the following procedure:

$$D_x^{n+1}=\mathrm{e}^{-\frac{\sigma_z\Delta t}{\varepsilon_0}}D_x^n+F_x^{n+1}-\mathrm{e}^{-\frac{\sigma_z\Delta t}{\varepsilon_0}}F_x^n-$$
$$\frac{\varepsilon_0^2}{\sigma_z^2\Delta t}\left(\frac{\sigma_z\Delta t}{\varepsilon_0}-1+\mathrm{e}^{-\frac{\sigma_z\Delta t}{\varepsilon_0}}\right)\frac{\partial}{\partial z}H_y^{n+\frac{1}{2}}+$$
$$\frac{\varepsilon_0^2}{\sigma_z^2\Delta t}\left(1-\frac{\sigma_z\Delta t}{\varepsilon_0}\mathrm{e}^{-\frac{\sigma_z\Delta t}{\varepsilon_0}}+\mathrm{e}^{-\frac{\sigma_z\Delta t}{\varepsilon_0}}\right)\frac{\partial}{\partial z}H_y^{n-\frac{1}{2}}. \quad (17)$$

The updated equations of the other field components and the auxiliary variables can be obtained by employing the same procedure. The auxiliary and the field variables updated equations in the PML regions are (16) and (17), respectively. The updated procedure can be described as follows:

Step 1 Update the field components D_x, D_y, D_z, B_x, B_y and B_z according to (17).

Step 2 Update the field components F_x, F_y and F_z according to (16).

To demonstrate the computational efficiency in theory, the number of auxiliary variables, coefficients, multiplications/ divisions (M/D) and additions/subtractions (A/S) of different PML implementations are employed for comparison. As shown in Table 1, the details of them are listed.

It can be observed from Table 1 that compared with the CT-MZT-PML, the A/S decreases by 33.3%, resulting in the highest computational efficiency among these implementations. In addition, it can be easily founded that the CT-MZT-PML shows the best performance among the existed previously works. For further comparison, Table 2 shows M/D, A/S and the exponential manipulation in the coefficients among the CT-MZT-PML and the proposed scheme. The details of the coefficients can be founded in [11,12].

Table 1 Number of M/D, A/S and coefficients used by different implementations

PML algorithm	Auxiliary variable	M/D	A/S	Coefficient
UPML	2	6	8	8
SC-PML	2	6	8	8
LI-PML	2	6	7	6
OR-PML	2	6	7	6
CT-ADE-PML	1	4	6	4
CT-BZT-PML	1	4	6	4
CT-MZT-PML	1	4	6	2
ETD-PML	1	4	4	2

Table 2 Number of M/D, A/S and exponential manipulation in the coefficients in CT-MZT-PML and ETD-PML

PML algorithm	M/D	A/S	Exponential manipulation
CT-MZT-PML	8	6	4
ETD-PML	8	4	3

Through the comparison, an additional exponential manipulation and two external A/Ss can be decreased by employing the proposed scheme which verifies the computational efficiency in theory.

3. Numerical examples

To validate the effectiveness of the proposed ETD-PML, numerical examples including the PEC sphere model and the patch antenna model are introduced. A PC with Intel Core$^{\mathrm{TM}}$ i7-8700K 3.20 GHz and 128 GB DDR4 (2666 MHz) is employed to implement the algorithms.

3.1 PEC sphere model related RCS problems

The absorbing performance and RCS obtained by different PML algorithms are evaluated through the PEC sphere model, as shown in Fig. 1. The PEC sphere model with the radius of R is located in the center of the FDTD domain. The rest part of the domain is filled with vacuum. The computational domain is with the size of $100\Delta x\times 100\Delta y\times 100\Delta z$. The incidence plane wave which is a modulated Gaussian pulse with the bandwidth and center frequency of 1.25 GHz propagates along the negative side of the x-direction. The size of the yOz incidence plane wave is a square with $100\Delta y\times 100\Delta z$ in the y- and z-directions. To observe the reflection wave of the PML regions with different incident angles, four observation points are selected which are located at (1, 1, 1), (1, 1, 25), (1, 1, 50) and (0,

50, 25). At the boundaries of the computational domain, 10-cell-PML is employed to absorb the outgoing waves.

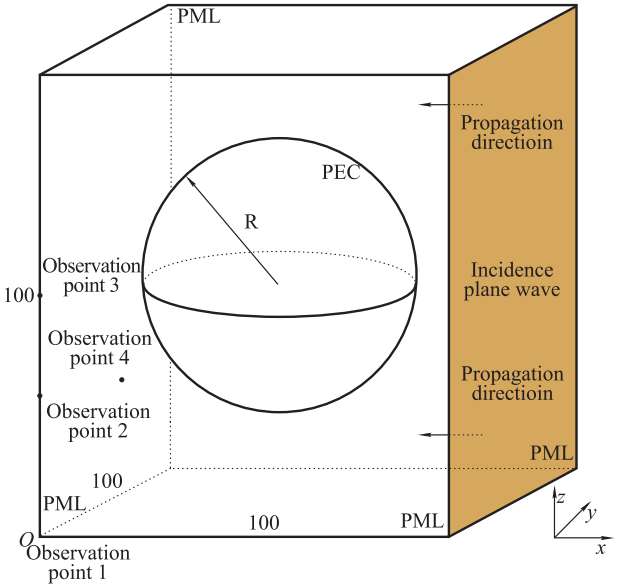

Fig. 1 Sketch of the PEC sphere model in the computational domain

The uniform mesh size with $\Delta x = \Delta y = \Delta z = \Delta = 2.5$ mm is employed. The time step can be obtained by the corresponding relationship as 4.81 fs [3]. Within the PML regions, the parameters are chosen according to the fourth order polynomial criterion to obtain the best absorbing performance. To illustrate the effectiveness of the proposed scheme, the UPML, SC-PML, LI-PML, OR-PML, CT-ADE-OPML, CT-BZT-PML, CT-MZT-PML are employed for comparison. According to the fourth order polynomial criterion adopted in this paper, m should be scaled below 4 at the integer. The parameters of the ETD-PML are selected as $m = 3$ and $R_0 = 0.001\%$, where m is the order of the polynomial. R_0 is the reflection coefficient along the vertical direction of the PML region, defined as

$$R_0 = \exp\left(-\frac{2\sigma_{\max}h}{(m+1)\varepsilon_0 c}\right) \tag{18}$$

where $\sigma_{\max}$ is the maximum permittivity of the PML region which is selected by the try and error approach; h is the thickness of the PML region; c is the speed of light. The parameters of UPML, SC-PML, CT-ADE-PML, CT-BZT-PML, LI-PML are $m = 2$ and $R_0 = 0.001\%$ [15]. The CT-MZT-PML and OR-PML are with the parameters of $m = 2$ and $R_0 = 0.01\%$.

In order to evaluate the absorbing performance of the PML regions, the relative reflection error is carried out in the time domain, which can be defined as

$$R_{dB}(t) = 20\lg\left|\frac{E_x^T(t) - E_x^R(t)}{E_{x\max}^R(t)}\right| \tag{19}$$

where $E_x^T(t)$ is the test solution which can be observed directly from the observation point; $E_x^R(t)$ is the reference solution which can be obtained by enlarging the computational domain to $200\Delta x \times 200\Delta y \times 200\Delta z$ and terminating by 32-cell-PML. During the calculation of the reference solution, the reflection wave of the computational domain can be ignored.

Firstly, the PEC sphere model with the radius of 100 mm is calculated. Thus, the radius of sphere is discretized as 40 cells. To further investigate the absorbing performance of the PML regions, the corner which shows the worst performance in the previously works is calculated by the same procedure [16]. As shown in Fig. 2, it can be also calculated that the maximum relative reflection errors (MRREs) in observation point 1 of the UPML, SC-PML, LI-PML, OR-PML, CT-ADE-PML, CT-BZT-PML, CT-MZT-PML and ETD-PML are -67.2 dB, -69.8 dB, -69.8 dB, -69.8 dB, -69.8 dB, -69.8 dB, -77.1 dB and -65.9 dB. It can be observed that the RREs of SC-PML, LI-PML, OR-PML, CT-ADE-PML and CT-BZT-PML are overlapped, indicating that the afore-mentioned algorithms hold the same absorbing performance. The CT-MZT-PML has the best absorbing performance. The absorbing performance of the ETD-PML is the worst. Although the absorbing performance of the ETD-PML is inferior among these implementations, it can be still employed in practical engineering (usually below -40 dB) [17]. It can be observed that the proposed scheme has advantages in terms of computational efficiency, computational time, occupied memory, MRRE and time reduction of the proposed implementations are shown in Table 3.

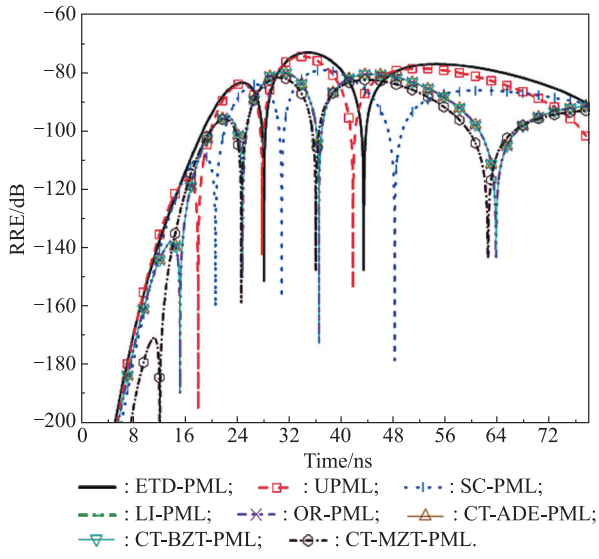

Fig. 2 RRE versus time obtained by different PML algorithms

It can be concluded from Table 3 that although the proposed ETD-PML has the worst absorbing performance

among the above-mentioned implementations, the computational efficiency and the computational resources can be significantly reduced compared with the other implementations. Compared with the conventional SC-PML and UPML algorithms, the computational efficiency of the ETD-PML scheme reduces by 29.5%, 30.6% and the occupied memory decreases by 1.0 MB. The ADE-PML and BZT-PML hold the same computational efficiency with the time reduction of 22.2% and 22.6%. Thus, the proposed scheme is suitable for the fast speed simulation among the above-mentioned implementations.

Table 3 Computational time, occupied memory, MRRE and time reduction with different PML implementations

PML algorithm	Memory/MB	Computational time/s	MRRE/dB	Time reduction/%
SC-PML	8.2	198.6	−69.8	—
UPML	8.2	201.7	−67.2	−1.5
LI-PML	8.0	185.1	−69.8	6.8
OR-PML	8.1	182.9	−69.8	7.9
CT-ADE-PML	7.6	154.5	−69.8	22.2
CT-BZT-PML	7.6	153.7	−69.8	22.6
CT-MZT-PML	7.7	164.1	−77.1	17.4
ETD-PML	7.2	140.0	−65.9	29.5

To observe the absorbing performance with different incident angles, MRRE versus observation points with different PML implementations is shown in Fig. 3.

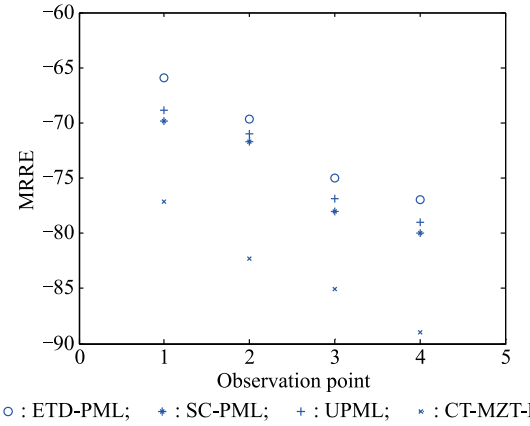

Fig. 3 MRRE versus observation points with different PML implementations

To clarify the demonstration of the absorbing performance versus different angles, four implementations are selected. As shown in Fig. 3, it can be concluded that the absorbing performance at the edge of the domain is worse compared with that at the surface. Among observation points 1, 2 and 3, the MRRE decreases with the increment of the distance between the sphere model and the observation point. Fig. 4 shows the absorbing performance of different implementations with different thickness.

As shown in Fig. 4, the MRRE decreases with the increment of the PML thickness. Thus, it can be concluded that the absorbing performance will be enhanced by employing the thicker PML layers. In the practical problems, the cells per wavelength (CPW) is regarded as one of the most important parameters. The CPW can be regarded as the ratio of wavelength to the cell size. Thus, the CPW versus the absorbing performance is testified. To satisfy the courant condition, the CPW is with the minimum value of 12. Fig. 5 shows the CPW versus the MRRE with different implementations. Through the resultants, it can be observed that the absorbing performance becomes worse with the increment of the CPW. The reason is that the mesh size becomes smaller with the increment of the CPW. Meanwhile, the PML becomes thick with the larger CPW. As illustrated in the previously example, the absorbing performance becomes worse with the decrement of the PML thickness. Thus, such phenomenon occurrs.

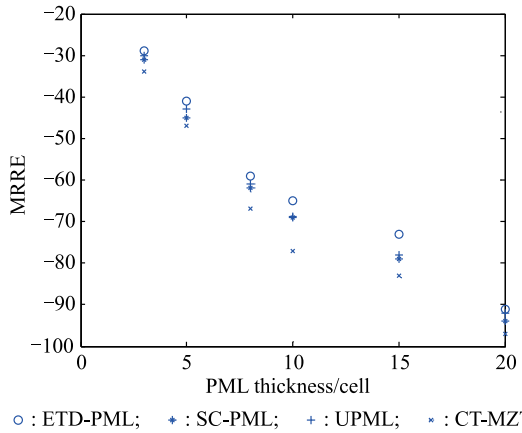

Fig. 4 Absorbing performance of different implementations with different thickness

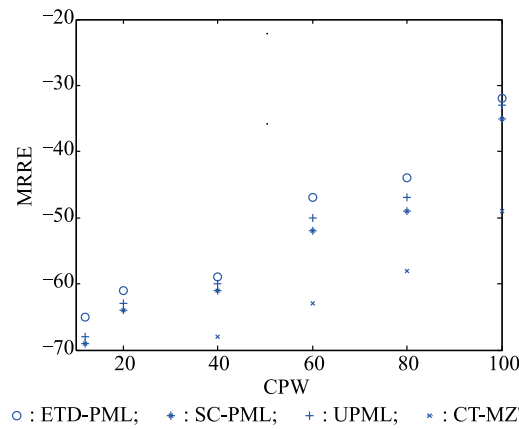

Fig. 5 CPW versus MRRE with different implementations

The accuracy and the effectiveness of the proposed scheme in the frequency domain are reflected by the RCS parameters. Fig. 6 shows the RCS parameters of the PEC sphere obtained by employing different PML algorithms.

It can be observed that the RCS parameters obtained by different PML algorithms are overlapped, indicating that

the afore-mentioned PML algorithms have the same accuracy in calculating RCS problems.

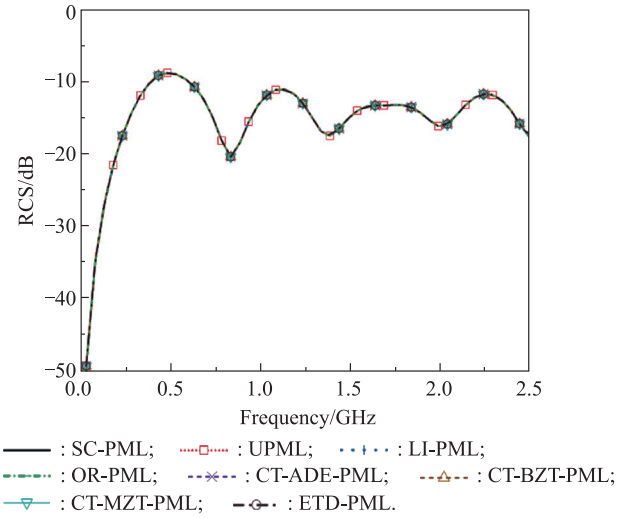

Fig. 6 RCS of the PEC sphere model obtained by different PML algorithms in the frequency domain

To investigate the computational efficiency versus sizes, 40-cell-sphere inside several domains including $100\Delta x \times 100\Delta y \times 100\Delta z$, $90\Delta x \times 90\Delta y \times 90\Delta z$ and $200\Delta x \times 200\Delta y \times 200\Delta z$ are considered. The ETD-PML and the SC-PML are employed to terminate the boundaries. The RCS of the sphere model within different domains are shown in Fig. 7. It can be observed that they are almost overlapped, indicating that the ETD-PML is with the considerable accuracy in different domains. The computational efficiency of different computational domains are shown in Table 4. It can be concluded that the computational efficiency can be improved significantly with larger domains. The reason is that the number of operators can be decreased significantly in larger domains by employing the proposed scheme resulting in the improvement of efficiency.

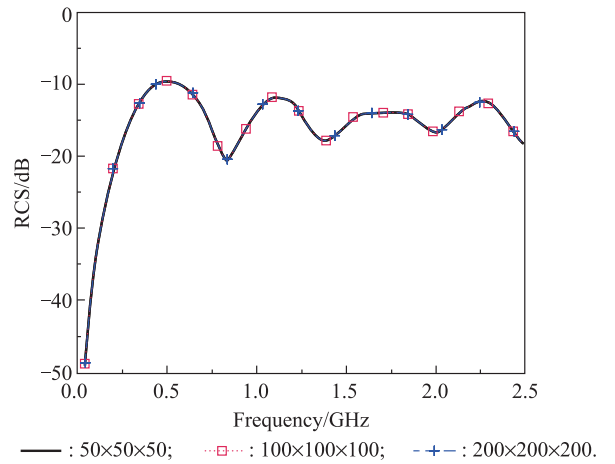

Fig. 7 RCS of the PEC sphere model obtained by ETD-PML with different domains

In conclusion, although the absorbing performance of the proposal in inferior to the other schemes, the proposed ETD-PML holds the least occupied memory and the computational time. Thus, the ETD-PML is suitable for the simulation of the RCS relevant problems, especially in large computational domains.

Table 4 Computational time, occupied memory, and time reduction of ETD-PML and SC-PML in different domains

Parameter	Size		
	90×90×90	100×100×100	200×200×200
Memory SC-PML/MB	6.7	8.2	20.9
Memory ETD-PML/MB	6.0	7.2	17.4
Time SC-PML/s	94.7	198.6	784.2
Time ETD-PML/s	79.1	140.0	491.6
Reduction/%	16.5	29.5	37.3

As can be concluded from Fig. 6 and Fig. 7 that the RCS is concentrated from -10 dB to 20 dB. The computational accuracy should be testified through low RCS structures. Thus, the radius of the sphere is chosen as 12.5 mm (5 cells) to further demonstrate the effectiveness. Fig. 8 shows the RCS of the sphere model with the radius of 12.5 mm. It can be observed that the curves are overlapped, indicating that the proposed algorithm can maintain higher accuracy in the calculation of the low RCS model.

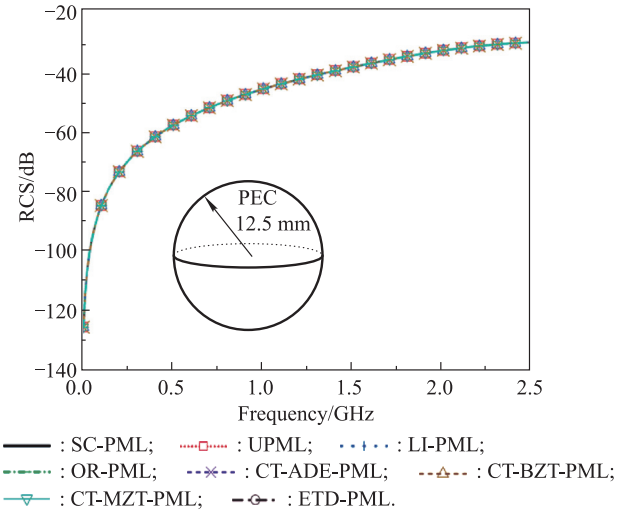

Fig. 8 RCS of the 12.5 mm PEC sphere model obtained by different PML algorithms in the frequency domain

Instead of the monostatic RCS, the bistatic RCS is regarded as one of the most important parameters. Thus, the bistatic RCS is investigated through the PEC sphere model at 2.5 GHz. Fig. 9 and Fig. 10 show the bistatic RCS of 100 mm and 12.5 mm PEC sphere model versus degree at 2.5 GHz, respectively. It can be observed that the curves are almost overlapped, indicating the considerable computational accuracy.

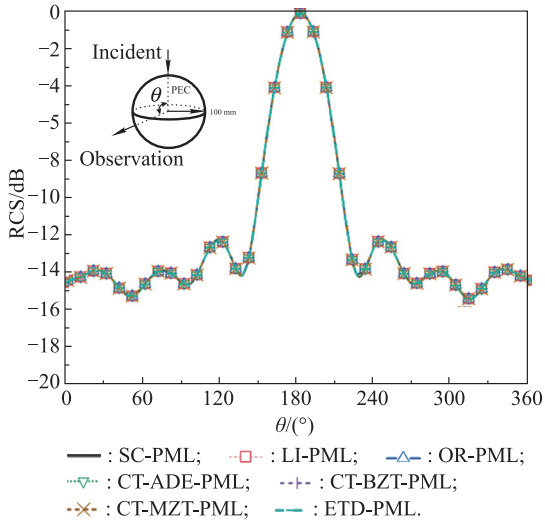

Fig. 9 Bistatic RCS of the 100 mm PEC sphere model versus degree obtained by different PML algorithms in 2.5 GHz

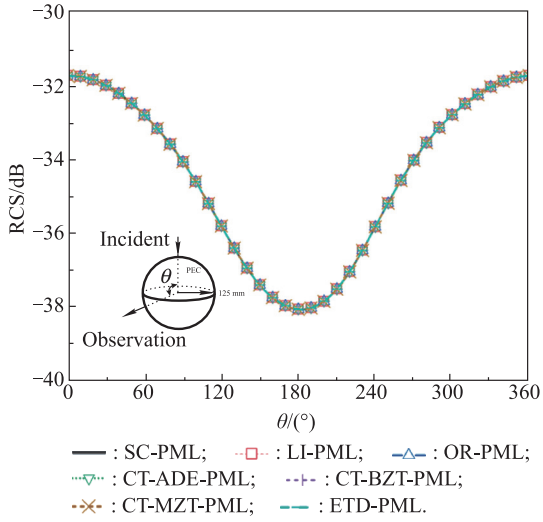

Fig. 10 Bistatic RCS of the 12.5 mm PEC sphere model versus degree obtained by different PML algorithms in 2.5 GHz

3.2 Patch antenna related RCS problems

To further demonstrate the effectiveness of the proposed ETD-PML, a patch antenna model is carried out as shown in Fig. 11.

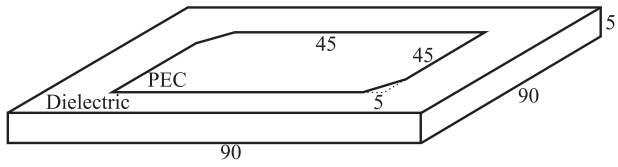

Fig. 11 Model patch antenna structure

The antenna is with 90 mm×90 mm×5 mm in x-, y- and z-directions. The substrate is the dielectric with $\varepsilon_r = 3.38$. The cut angles are with the shape of triangles with the sides length of 5 mm. The material of the patch can be seemed as the PEC. To simulate the RCS of the antenna and evaluate the absorbing performance, a computational domain with the size of $100\Delta x \times 100\Delta y \times 40\Delta z$ is employed. The antenna model is located at the center of the domain. The boundaries of the domain are terminated by 10-cell-PML, as shown in Fig. 12. The incidence plane wave which is the modulated Gaussian pulse propagates along the negative direction of the z-direction. The plane wave in the xOy plane is a square which has the side length of 500 mm both in the x- and y-directions. The modulated Gaussian pulse is with the center frequency of 2.5 GHz and bandwidth of 0.5 GHz. The mesh sizes are chosen as $\Delta x = \Delta y = 5$ mm and $\Delta z = 1$ mm. The time step can be obtained by 1.9 fs.

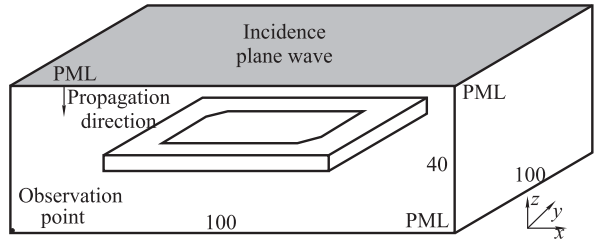

Fig. 12 Sketch picture of the patch antenna domain

Following the same steps, the resultants can be obtained. The parameters of the PML schemes are the same as the numerical example above. Fig. 13 shows the RRE versus time obtained by different PML algorithms.

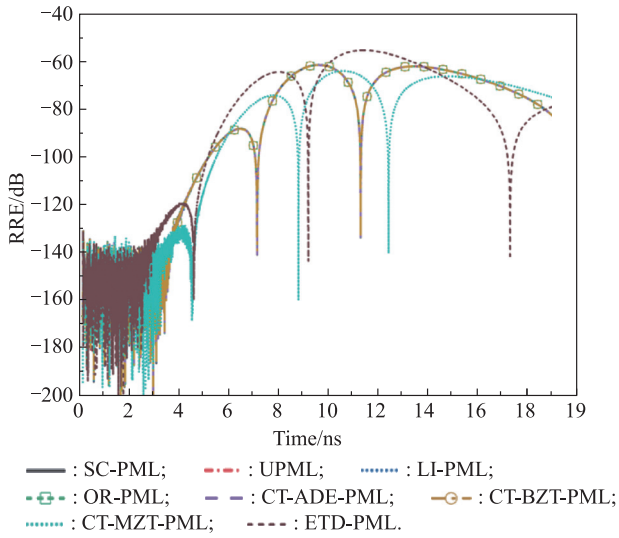

Fig. 13 RRE versus time obtained by different PML algorithms

It can be observed from Fig. 13 that the MRREs of the SC-PML, LI-PML, OR-PML, CT-ADE-PML, CT-BZT-PML, CT-MZT-PML and ETD-PML are −61.2 dB, −61.2 dB, −61.2 dB, −61.2 dB, −63.0 dB, −56.6 dB and −64.9 dB, respectively. The RREs of SC-PML, LI-PML, OR-PML, CT-ADE-PML and CT-BZT-PML are overlapped, indicating good agreement of the afore-mentioned

algorithms. On the whole, good absorbing performance of both proposed methods has been achieved. Table 5 shows the computational time, memory and MRRE with different PML implementations. It can be concluded that the ETD-PML can obtain the highest computational efficiency among above mentioned schemes.

Table 5 Computational time, occupied memory, MRRE and time reduction with different PML implementations

PML algorithm	Memory/MB	Computational time/s	MRRE/dB	Time reduction/%
SC-PML	6.8	159.2	−61.2	—
UPML	6.8	161.7	−59.4	−1.5
LI-PML	6.7	140.1	−61.2	12.0
OR-PML	6.7	140.0	−61.2	12.1
CT-ADE-PML	5.9	129.2	−61.2	18.8
CT-BZT-PML	5.9	129.8	−61.2	18.5
CT-MZT-PML	6.1	132.5	−63.0	16
ETD-PML	5.3	116.7	−56.6	26.7

It can be observed from Fig. 14 that the RCS obtained by different PML algorithms are overlapped. Thus, the aforementioned PML schemes almost have the same computational accuracy.

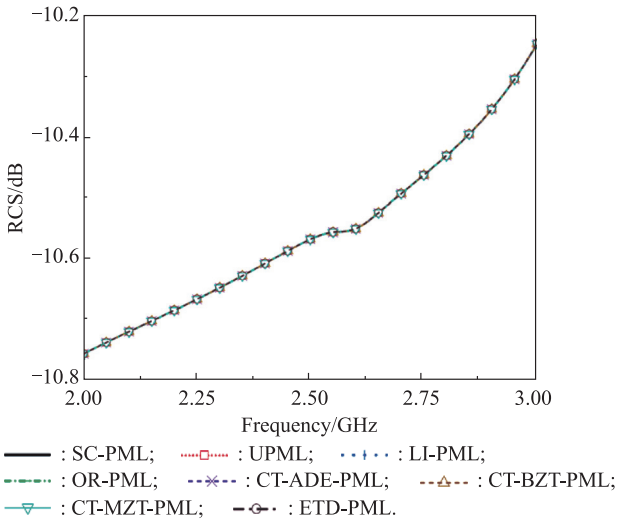

Fig. 14 RCS of the patched antenna obtained by different PML algorithms

4. Conclusions

Based on the ETD-FDTD method, an ESC-PML is proposed. Numerical examples including the PEC sphere model and the patch antenna model are carried out. The results demonstrate that although the absorbing performance of the proposed ETD-PML is inferior compared with the other implementations, the computational efficiency and the occupied memory can be significantly reduced. The RCS parameters are overlapped, indicating that the proposal can obtain considerable computational accuracy. In conclusion, the proposed ETD-PML is suitable for the large domain, fine structure relevant RCS problems.

References

[1] KNOTT E F, SHAEFFER J F, TULEY M T. Radar cross section. 2nd ed. New York: Artech House, 1993.
[2] SONG J, LU C C, CHEW W C. Multilevel fast multipole algorithm for electromagnetic scattering by large complex objects. IEEE Trans. on Antennas & Propagation, 1997, 45(10): 1448 – 1493.
[3] TAFLOVE A, HAGNESS S C. Computational electrodynamics: the finite-difference time-domain method. 3rd ed. Boston and London: Artech House, 2005.
[4] BERENGER J P. A perfectly matched layer for the absorption of electromagnetic waves. Physics of Plasmas, 1994, 114(2): 185 – 200.
[5] CHEW W C, WEEDON W H. A 3D perfectly matched medium from modified Maxwells equations with stretched coordinates. Microwave and Optical Technology Letters, 1994, 7(13): 599 – 604.
[6] RAMADAN O. Auxiliary differential equation formulation: an efficient implementation of the perfectly matched layer. IEEE Microwave and Wireless Components Letters, 2003, 13(2): 69 – 71.
[7] LI J, DAI J. Z-transform implementations of the CFS-PML. IEEE Antennas and Wireless Prapagation Letters, 2006, 5(1): 410 – 413.
[8] SULLIVAN D M. Z transform theory and the FDTD method. IEEE Trans. on Antennas & Propagation, 1996, 44(1): 28 – 34.
[9] LI J, DAI J. Efficient implementation of stretched coordinate perfectly matched layer using DSP techniques. Electronics Letters, 2006, 42(17): 953 – 954.
[10] RAMADAN O. General ADE formulations of SC-PM for modelling multiterm dispersive FDTD applications. Electronics Letters, 2011, 47(20): 1122 – 1124.
[11] JIANG H L, CUI T J, WU L T, et al. Efficient implementations of SC-PML for arbitrary media using DSP techniques. IEEE Trans. on Electromagnetic Compatibility, 2019, 61(3): 962 – 965.
[12] JIANG H L, CUI T J. Simple PML implementation for finite-difference time-domain method. Electronics Letter, 2018, 54(16): 988 – 990.
[13] WEEDON W H, RAPPAPAPORTC M. A general method for FDTD modeling of wave propagation in arbitrary frequency-dispersive media. IEEE Trans. on Antennas & Propagation, 1997, 45(3): 401 – 410.
[14] XU Z S, MA X K. Integral-based exponential time differencing algorithms for general dispersive media and the CFS-PML. IEEE Trans. on Antennas & Propagation, 2012, 60(7): 3257 – 3264.
[15] LI J X, SHI X Y. 2-D unconditionally stable CFS-PML based on CNDG for truncating unmagnetized plasma media. IEEE Microwave and Wireless Components Letters, 2017, 27(4): 323 – 325.
[16] GEDNEY S D. An anisotropic perfectly matched layer-absorbing medium for the truncation of FDTD lattices. IEEE Trans. on Antennas & Propagation, 1996, 44(12): 1630 – 1639.
[17] JIANG H L, WU L T, ZHANG X G, et al. Computationally efficient CN-PML for EM simulations. IEEE Trans. on Microwave Theory Techniques, 2019, 67(12): 4646 – 4655.

Biographies

NIU Liqiang was born in 1980. He received his B.Sc. degree and M.Sc. degrees in the School of Information Science and Engineering from Shandong University of Science and Technology and the School of Physics Science and Information Technology from Liaocheng University, respectively. He is currently working towards his Ph.D. degree in the School of Electronic and Information Engineering at Beihang University. His current research interests include computational electromagnetics, and electronic counter-measures.
E-mail: liqiangniu@126.com

XIE Yongjun was born in 1968. He received his B.Sc., M.Sc., and Ph.D. degrees in electronic engineering from Xidian University, Xian, China, in 1990, 1993, and 1996, respectively. From March 1998 to November 1999, he joined the University of Texas at Dallas, Dallas, TX, USA, as a postdoctoral research associate. From December 1999 to October 2001, he was a postdoctoral research associate with Duke University. In October 2001, he joined Xidian University as a professor. In 2004, he was supported by the Program for the New Century Excellent Talents launched by Ministry of Education, China. Since 2009, he is currently a professor with Beihang University. His research interests include computational electromagnetics, electromagnetic theory, microwave technology, antenna theory, microwave components, terahertz technology and mobile telecommunication.
E-mail: yjxie@buaa.edu.cn

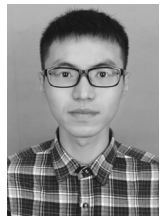

JIANG Haolin was born in 1989. He received his B.Sc. degree in the School of Electronic Engineering from Tianjin University of Technology and Education in 2012, and his M.Sc. degree in the School of Electronics and Information Engineering from Tianjin Polytechnic University in 2016. He is currently working toward his Ph.D. degree in the School of Information Science and Engineering at Southeast University, Nanjing. His current research interests include computational electromagnetics and parallel computing.
E-mail: haolinjiang.cem@gmail.com

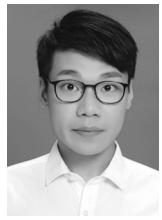

WU Peiyu was born in 1994. He received his B.Sc. degree and M.Sc. degrees in the School of Electronics and Information Engineering from Tianjin Polytechnic University in 2016 and 2019, respectively. He is currently working towards his Ph.D. degree in the School of Electronic and Information Engineering at Beihang University, Beijing. His current research interests include the computational electromagnetics, antenna and microwave components.
E-mail: wupuuu@yahoo.com